Spin-Polarized Density Functional Theory Study of Reactivity of Diatomic Molecule on Bimetallic System: The Case of O_2 Dissociative Adsorption on Pt Monolayer on Fe(001)†

Mary Clare Sison Escano, Hiroshi Nakanishi, and Hideaki Kasai*

Department of Precision Science & Technology and Applied Physics, Osaka University 2-1 Yamadaoka Suita, Osaka 565-0871, Japan

Received: April 2, 2009; Revised Manuscript Received: May 27, 2009

The energetics of O_2 adsorption and dissociation are discussed in terms of 6D potential energy surface based on spin-polarized density functional theory calculations that predict O_2 access to both molecular and dissociative chemisorption wells with no obvious barriers. Specifically, a molecularly chemisorbed state in a top-bridge-top (*t-b-t*) configuration is identified, and a "no barrier" dissociative adsorption over hollow site with the O−O axis spanning toward the bridge sites (*b-h-b*) is noted. Both the translation of O_2 from the molecular state (*t-b-t*) to the dissociated state on bridge and the direct nonactivated dissociative adsorption over the hollow sites (*b-h-b*) are likely pathways for O_2 dissociation. Interestingly, such O_2 reaction pathways are consistent with the density functional theory calculations and molecular beam experiments on O_2 dissociative adsorption on Pt(100)-(1 × 1). Modification of the electronic structure of the Pt surface due to the Fe substrate relevant for O_2 reactivity is discussed in an effort to provide insight into the experimentally discovered significant enhancement in electrocatalytic activity of Pt−Fe alloys for fuel cell applications.

Introduction

Considerably large research attention has been directed to the oxygen reduction reaction (ORR) catalyzed by Pt and Pt-based alloys because of its importance in many industrial and biological processes. For instance, the polymer electrolyte fuel cell (PEFC), an efficient and environmentally friendly power generator, has the ORR as one of its surface electrode reactions (i.e., $^1/_2O_2 + 2H^+ + 2e^- = H_2O$ (cathodic reaction)). The large cathodic overpotential loss attributed to the slow kinetics of ORR is the primary technical challenge that should be addressed to make PEFC economically viable.[1] On the basis of detailed density functional theory (DFT) calculations,[2] the origin of overpotential was attributed to the stability of surface intermediates (adsorbed O and OH) at potentials close to equilibrium, which then limits or enhances proton/electron transfer to such adsorbed species. In addition to this, a volcano-shaped relationship between the rate of cathode reaction and oxygen adsorption energy was established, which shows: (1) why Pt is the best catalyst so far, (2) that there is still room for improvement for Pt catalytic activity, and (3) how alloying can be used to achieve part 2.

During the past decades, PEFC cathode catalyst design has already involved the development of Pt-based alloys, which are believed to be the reservoir of more active ORR catalysts with less Pt loading and with greater stability.[3−8] Therefore, various Pt-alloy catalysts have been prepared, and their electrocatalytic activity has been evaluated. In general, platinum-3d transition metal, M (M = Cr, Ni, Co, and Fe) alloys were reported to have exhibited relatively higher cathode activity for ORR than pure Pt.[3−6] The enhancement factor, however, varies on the basis of the alloying metal, M, and the type of Pt-M alloys. For the Pt_3M type, Pt_3Co is recently reported to have an ORR activity improvement factor of 3 compared with the "standard" supported Pt catalyst,[9] whereas a series of binary PtM alloys (M = Cr, Mn, Co, Ni) supported on carbon have been reported to produce an enhancement in the kinetics of ORR by a factor of 3−5.[10] The Pt−Fe alloys, however, which include those of Pt_3Fe, PtFe, and $PtFe_3$ types, have shown a highly improved electrocatalytic activity up to 25 times over pure Pt.[11] This is a unique behavior for Pt−Fe alloys, which is attractive for the investigation of the mechanism of significant enhancement in electrocatalytic activity. Moreover, Pt_3Fe is known to be a good representative system for Pt_3M types because of its stability in the electrochemical environment.[9]

Clearly, the various types of Pt-alloys and their different electrocatalytic behaviors and the various ORR mechanisms proposed[12−15] make the formulation of bases for the catalytic enhancement across different Pt-alloy systems difficult. However, the complexities are somehow curtailed by the commonly observed segregation of Pt atoms to the surface in most Pt-alloy systems, forming a pure Pt atomic layer across many types of Pt-alloys.[16] Here we modeled the Pt-enriched layer on Pt−Fe bulk alloys formed as a result of Pt segregation to the surface using the Pt monolayer on the Fe(001) system (Pt/Fe). In fact, on the basis of experiment,[11] in all Pt−Fe alloy types and composition, it is found that the catalyst surface is always covered by pure Pt layer under PEFC operating conditions. With regard to the catalytic enhancement mechanism, typically, one resorts to two major mechanisms for the improvement of ORR of Pt-alloys: (1) geometrical changes caused by alloying (i.e., decrease in Pt−Pt bond distance[3]) and (2) electronic (increase in Pt-d electron vacancy[5] or shift in the Pt d-band center position relative to the Fermi level[9]). In this study, the change in surface electronic property of Pt due to the Pt−Fe interaction is seen to be more appropriate. Also, we capitalize on the recently established ORR mechanism, which assigns O−O bond scission in O_2, O_2H, or H_2O_2 as the rate-limiting step for surface with weaker O-atom binding and the OH removal via hydrogenation as the rate limiting step for surface with stronger O-atom binding.[17] It is known that oxygen tends to bind weakly to Pt-

† Part of the "Vincenzo Aquilanti Festschrift".

* Corresponding author. E-mail: kasai@dyn.ap.eng.osaka-u.ac.jp.

10.1021/jp9030267
Published on Web 07/09/2009

based alloys, and so the O−O bond scission mechanism is more appropriate in this study.

Next, because a decrease in dissociative adsorption energy of oxygen is often regarded to result in an increase in the O_2 dissociation barrier,[18] it is then thought that the O_2 dissociation barrier height on Pt-alloys and Pt-bimetallic mixtures (if we consider segregation of Pt to surface) would mostly likely be higher than that on pure Pt.[19] Therefore, the optimal Pt-based alloy ORR catalyst should strike a balance between O−O splitting and O−H bond-making activity, which may be achieved by a small decrease in the oxygen binding energy on the surface, E_b, quantified to be within the range $0 < E_b < 0.5$ eV on the basis of the volcano-shaped plot of the rate of cathode reaction versus oxygen adsorption energy discussed previously. Our previous study on atomic O chemisorption on Pt/Fe shows that the oxygen atom binds less to such a bimetallic system than to the corresponding pure metal slab, Pt(100)-(1 × 1), by ∼0.30 eV.[20] This fits perfectly in the volcano-type plot, however, the significantly large catalytic enhancement reported[5] is way beyond what one should expect for a 0.30 eV difference in oxygen binding energy. For instance, a 0.38 eV difference in oxygen binding energy between pure Pt and Pt_3Co based on DFT[6] resulted in an enhancement factor of just around 2 to 3.[9] Therefore, we investigated the O_2 reactivity on model bimetallic system, Pt/Fe, in comparison with that of the corresponding pure metal Pt(100)-(1 × 1) using ab initio DFT calculations. Here we determined the most probable O_2 reaction pathways and, more importantly, the absolute values for activation barriers for O_2 dissociation by carefully mapping out the 6D potential energy surface (PES). Changes in the electronic structure of the Pt surface are carried out using density of states analysis.

The small lattice mismatch between the Pt monolayer and the Fe substrate (0.5%)[21] rules out the role of strain in the modification of the electronic structure of the Pt surface and therefore allows simplification of the analysis of O_2 reactivity on the model bimetallic system by focusing solely on metal−metal interaction.

2. Computational Method

The first principles calculation performed in this study is based on spin-polarized total energy calculations within the DFT[22,23] framework using projector augmented wave (PAW) method[24,25] and plane-wave basis set implemented in the Vienna ab initio simulation program (VASP).[26−29] The spin-polarized version of the program accounts for the magnetic moment of O and ferromagnetic character of Fe. The PAW method was used instead of the pseudopotential technique because the latter is known to produce the wrong ordering of magnetic states of bulk Fe[30] The generalized gradient approximation (GGA) of Perdew, Burke, and Ernzerhof (PBE)[31,32] was used for the exchange-correlation functional because GGA is known to predict the correct ground state of Fe.[30,33] Brillouin-zone integrations were performed on a grid of (4 × 4 × 1) Monkhorst-Pack k points using Methfessel−Paxton smearing[34] of $\sigma = 0.2$ eV. The substrate is modeled by a five-layer slab in a (2 × 3) unit cell, and each slab is separated by ∼12.0 Å of vacuum. The unit cell size is large enough to avoid O_2 interactions between neighboring unit cells. The Pt atoms are pseudomorphically laid on the Fe substrate, forming the Pt monolayer. The calculated equilibrium lattice constants of 3.980 and 2.834 Å for Pt and Fe, respectively, are in excellent agreement with other DFT-GGA calculations.[35,36] We used the lattice parameter for Fe for all calculations. For atomic and molecular oxygen, a 400 eV cutoff energy yields a O_2 bond length of 1.235 Å and a dissociation energy of 5.67 eV, which is higher than the experimental value of 5.23 eV[37] but in agreement with other DFT calculations, 5.64[9] and 5.73 eV.[38] The atomic O binding energy on the corresponding pure Pt(100)-(1 × 1) (−4.18 eV relative to free oxygen atom) is in excellent agreement with Deskins et al. DFT calculations (−4.21 eV)[39] and the molecularly adsorbed O_2 binding energy on relaxed Pt(100)-(1 × 1) (−1.43 eV) are comparable to the thermal desorption experiment (TDS) result (−1.55 eV).[40] Because TDS gives an effective barrier for oxygen desorption, which includes (in addition to pure adsorption energy) the barrier in going from the adsorbed configuration to gas-phase O_2 as well as the pairwise interaction between adsorbates, the stabilization energy arising from any of these factors can very well account for the discrepancy. The kinetic energy cutoff used is sufficient to converge the total energies of O_2/Pt/Fe(001) and O_2/Pt(100)-(1 × 1) systems to within 5 meV/atom. The slab is kept at its optimized configuration in all total energy calculations for O_2/Pt/Fe(001) and O_2/Pt(100)-(1 × 1) systems. In the optimizations, structural relaxations are terminated when the maximum force acting on each atom in the supercell drops below 0.005 eV/Å.

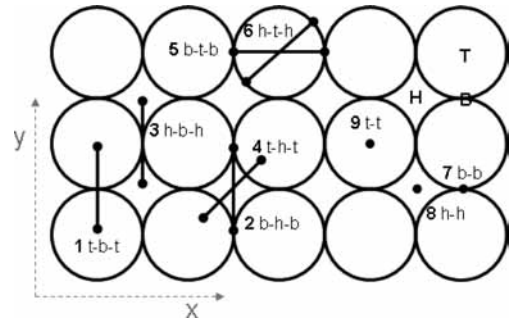

Figure 1. Reaction pathways explored in this study. Description of parallel trajectories (1−6) of O_2 is given in terms of the direction of the O−O axis and the position of the center-of-mass (c.m.) of the molecule (whether it is over bridge, hollow, or top). Vertical configurations (7−9) use O-atom position rather than its c.m. H, B, and T specify the hollow, bridge, and top sites.

3. Results and Discussion

3.1. Potential Energy Surface. First, we describe the different trajectories of O_2 in terms of the direction of the O−O axis and the position of the center-of-mass (c.m.) of the molecule (whether it is over bridge, hollow, or top site). For instance, *t-b-t* (channel 1 of Figure 1), refers to a configuration where the O_2 c.m. is over bridge site and the O−O axis spans toward top sites. Other trajectories include O−O axis perpendicular to the surface; in this case, we use the O atom position rather than its c.m. So, *b-b*, *h-h*, and *t-t* (channels 7−9) mean both O atoms fall directly over the same site. A total of nine trajectories are considered to account for the six degrees of freedom of the molecule sufficiently.

We explored each trajectory by calculating the total energy of the O_2/Pt/Fe system as a function of the height of the molecule from the surface (z) and the O−O bond length (r), where r is optimized at each explored O_2 c.m. distance from surface, z. The r and z step size are 0.1 and 0.2 Å, respectively. Such optimization of r is done to determine the deepest potential energy (PE) value at a given height and so is the corresponding most stable configuration of O_2. The r step size is chosen to be sufficiently small so that the accuracy of the calculated PE is ensured. Such method allows accurate descriptions of O−O bond length and binding energies upon O_2 approach to surface,

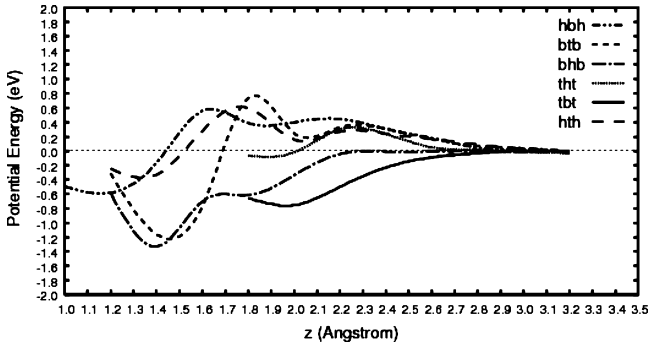

Figure 2. Variation of potential energy (PE) as O_2 approaches the Pt/Fe surface. The PE is determined with respect to separate O_2 and Pt/Fe slab. The total energies per trajectory are calculated as a function of the height of the molecule (z) and the O−O bond length (r), which is optimized at each height (z).

which are crucial in this study. The activation barrier for each channel is determined from the binding energy of the transition state (TS). All energies are potential energies with respect to the separate slab and O_2 ($E_b = E_{total} - E_{slab} - E_{gas\text{-}phase\ adsorbate}$). All trajectories or reaction pathways provide PE curves that may be further explored (Figure 2) to determine possible PE dependence on O_2 translation along x and y axes and rotation over hollow, bridge, and top sites. Specifically, pathways 1−3, as shown in Figure 1, explore PE dependence on O_2 translation. Pathways 4,2; 5,6; and 1,3 explore the rotational (azimuthal) dependence of PE on hollow, top, and bridge sites, respectively. Trajectories 7,8,9 are vertical configuration that can be used to explore the "cartwheel" rotational dependence of PE.

In Figure 2, we show the variation in PE along these reaction pathways. Perpendicularly oriented O_2 is very weakly bound, which is indicative of a very low Pt surface reactivity with O_2 arriving vertical, and so trajectories 7−9 were not included in the Figure. Bond scission is found to be unfavorable in these configurations on the bimetallic system (Pt/Fe) and in the corresponding pure metal. However, in the latter sections, we will relate initial sticking probability measurements of O_2 on pure metal to the adsorption and the possibility for steering from such unfavorable native configurations. Here the analysis of PES focuses on O_2 arriving with O−O axis parallel to the surface. Across all trajectories, the molecule enters at around 3.20 Å from the surface with a 1.235 Å bond length.

On the basis of the 1D PES in Figure 2, O_2 traverses both top-bridge-top (*t-b-t*) and bridge-hollow-bridge (*b-h-b*) without obvious barriers. It is interesting to note that these channels are the deepest local (−0.76 eV) and global (−1.38 eV) minima, which indicate that these are the most likely reaction pathways for O_2 in the bimetallic model system. In Pt(100)-(1 × 1), the same O_2 reaction pathway is determined. Figure 3 shows PE curves for the corresponding *t-b-t* (solid line) and *b-h-b* (dashed line) channels, which also give the deepest local (−1.30 eV) and global (−2.40 eV) minima, respectively.

In both systems, we found that the *t-b-t* is a molecular adsorption channel. The O_2 at this configuration on Pt/Fe is illustrated in Figure 4. The adsorbed O_2 is characterized by a bond length (r) of 1.37 Å and an O_2 c.m. distance (z) of 1.92 Å. The binding energy is −0.76 eV with respect to the gas-phase O_2. In addition, the magnetic moment of O is quenched. Relaxed calculations for O_2 at *t-b-t* configuration were also done, and no significant difference in geometry and binding energy of O_2 is observed. The O−O bond length is essentially the same, and the binding energy difference is just ∼0.01 eV.

In Pt(100)-(1 × 1), a molecularly chemisorbed O_2 in the same symmetric *t-b-t* position is noted and is characterized by a bond

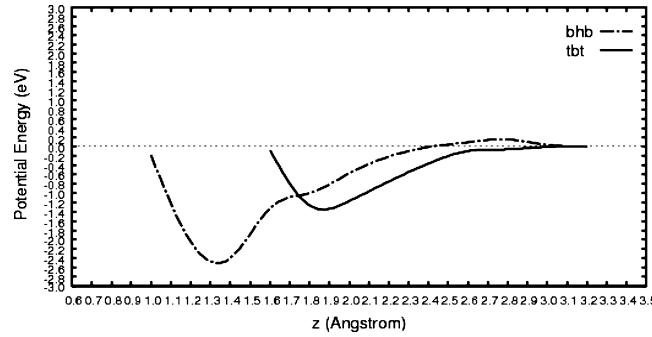

Figure 3. Variation of potential energy (PE) as O_2 approaches the Pt(100)-(1 × 1) surface in a *t-b-t* channel (solid line) and *b-h-b* channel (dashed line). The PE is determined with respect to separate O_2 and Pt/Fe slab. The total energies per trajectory are calculated as a function of the height of the molecule (z) and the O−O bond length (r) which is optimized at each height.

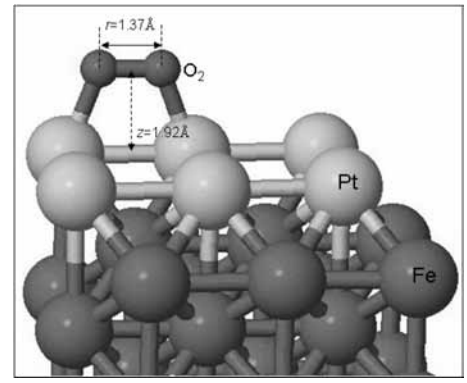

Figure 4. Geometry of O_2 at *t-b-t* configuration on Pt/Fe.

length (r) of 1.37 Å, an O_2 c.m. distance (z) of 1.84 Å, and a binding energy of −1.30 eV. The magnetic moment of oxygen is also quenched. On the basis of the bond length, binding energy, and the magnetic moment, this molecular state on pure Pt could be a nonmagnetic peroxo, O_2^{2-}. A molecular adsorption for O_2 at low incident energy (E_i) regime is predicted on the basis of the initial sticking probability (s_o) profile for O_2/Pt(100)-(1 × 1) from a molecular beam experiment (MBE).[41] In this regime, steep fall of s_o with increasing translational energy, E_i, indicates that the molecularly chemisorbed O_2 is a precursor to dissociative O_2 adsorption, whereas the subsequent rise in s_o with increasing E_i indicates opening up of another channel that is activated and direct. This opening up of activated the dissociative adsorption channel is also noted both in Pt/Fe and in Pt(100)-(1 × 1) on the basis of DFT in this work (Figures 2 and 3). The crossing point between the *t-b-t* curve and the *b-h-b* curve indicates a transition that is activated. A separate PES scanning corresponding to O_2 translation along x (i.e., transition from *t-b-t* to *b-h-b* channel) in Pt/Fe is conducted, this time fixing the y coordinate of the molecule while the energy of the system is minimized with respect to other degrees of freedom. Results that are shown in Figure 5 clarify the fact that the O_2 at the TS is higher in energy by ∼0.13 eV relative to the initial state (molecular adsorption at *t-b-t*). The translation of the molecule in this system along the x direction is indeed activated. The O−O bond length at TS is slightly stretched to 1.4 Å (r) with 1.80 Å (z) distance from surface. We call this O_2 translation toward dissociation in *b-h-b* a "surface dissociation" mechanism to differentiate it from direct dissociative adsorption paths.

The *b-h-b* channel yields the most stable oxygen adsorption, which is characterized by a binding energy of −1.38 eV (with respect to gas-phase O_2), an O−O distance (r) of 2.80 Å, and

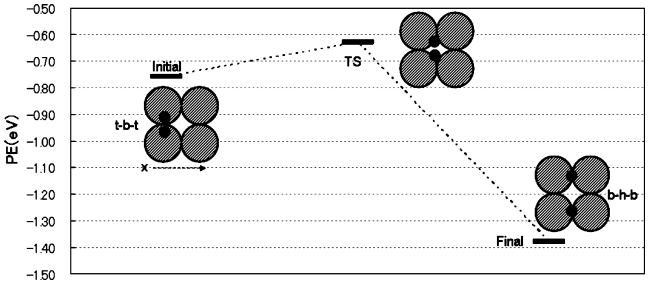

Figure 5. Sketch of initial, transition, and final states of O_2 on the Pt/Fe surface with the corresponding oxygen binding energy (with respect to gas-phase O_2). The dashed line is a guide for the eye.

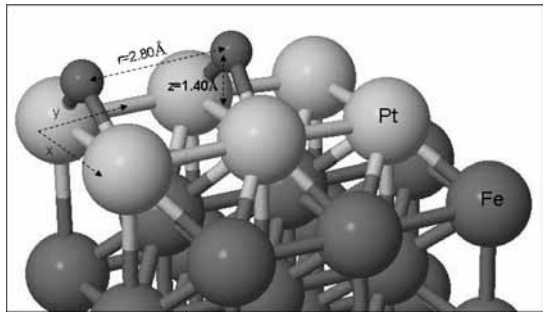

Figure 6. Geometry of dissociated oxygen following *b-h-b* configuration.

an O_2 c.m. distance from surface (z) of 1.40 Å. Given the bond length, this adsorbed oxygen is already in the dissociated state. The dissociation yields two oxygen atoms chemisorbed on two adjacent bridge sites, as further illustrated in Figure 6. For Pt(100)-(1 × 1), O_2 transition from *t-b-t* to *b-h-b* yields an activation barrier of ∼0.14 eV using the same PES scanning corresponding to O_2 translation along x as that of Pt/Fe, as previously discussed. Clearly, such transition from molecular adsorption on *t-b-t* to dissociation toward *b-h-b* is activated for both systems; then, first, we expect that O_2 most likely traverses the direct dissociative adsorption path (*b-h-b*) for the bimetallic system, which offers lesser activation barrier for O_2 dissociation. Also, the direct dissociative adsorption path (*b-h-b*) would most likely be the case for O_2 arriving at Pt(100)-(1 × 1), especially at higher O_2 translational incident energies. At lower incident energies, the molecule may be trapped in a molecular state,[41] which on the basis of our calculations and previous discussions, the most stable is identified over bridge (*t-b-t*). The *t-h-t* configuration also offers a molecularly chemisorbed state with much less binding than that of *t-b-t* configuration for both bimetallic (−0.07 eV) and pure metal (−0.95 eV). Such molecular state may allow steering (planar rotation) toward *b-h-b* (Figure 1) as well as *h-b-h* toward the most stable *t-b-t* molecular adsorption. For perpendicularly oriented molecules, the *b-b* configuration offers the most stable adsorption. However, the interaction with the surface is barely stable, and it resembles the gas-phase O_2. Both the *b-b* configuration and the *t-t* configurations may be steered (cartwheel rotation) toward *b-h-b* and *t-b-t* sites, respectively. A dynamical approach is needed to verify these possibilities. In the meantime, under moderate reaction conditions, the molecule is expected to traverse the direct dissociation path, here termed a "direct dissociation" mechanism. Under modest reaction conditions, the molecule traverses the "surface dissociation" path. The initial sticking probability at 123 and 300 K surface temperature, where Pt(100)-(1 × 1) is stable, is ∼0.4 ± 0.1 and ∼0.1, respectively,[40,42,43] which is qualitatively consistent with the above observations.

Moreover, on the basis of the crossing point of PE curves for molecular adsorption (*t-b-t*) and direct dissociative adsorption (*b-h-b*), which falls below the PE zero for both the bimetallic (Figure 2) and pure metal (Figure 3), increasing surface temperature should favor chemisorption rather than desorption. This is consistent with the X-ray photoelectron spectroscopy (XPS) of Norton et al., which shows peak characteristics of atomically adsorbed oxygen for O_2 adsorbed at (1 × 1) surface warmed to 300 K.[42]

Next, we note from Figures 2 and 3 that both the Pt/Fe and Pt(100)-(1 × 1) systems render no barrier O_2 molecular adsorption along *t-b-t*. However, in the *b-h-b* channel where direct dissociation occurs, a significant difference in both the activation barrier and the binding energy of dissociated oxygen is noted. Therefore, the study of the differences of the reactivity of the two systems can be focused on the surface reactivity with O_2 arriving horizontally in a *b-h-b* configuration. It is clear from the 1D PES in Figure 2 that no energy expense is required for O−O bond scission in Pt/Fe; however, in Figure 3, oxygen has to overcome an activation barrier of 0.16 eV to dissociate in pure Pt. In addition to this, it is significant to note that the binding of dissociated atomic oxygen on bridge is weaker in Pt/Fe as compared with the pure metal. Therefore, the bimetallic system yields both easy O_2 dissociation and weaker O atom binding on surface. In this, we trace the significant enhancement in electrocatalytic activity of Pt-enriched Pt−Fe alloys. The unique combination of easy O_2 activation, which is rate limiting in Pt-based alloy and Pt-bimetallic mixtures, and the weaker O atom binding on the surface explains the large enhancement in Pt electrocatalytic activity. A certain class of metal monolayer on metal substrates called "near surface alloys" has been found to exhibit the same behavior for H_2 dissociation.[44]

3.2. Changes in Pt Surface Electronic Structure. In determining the modification of electronic structure of Pt surface in Pt/Fe, we first employ the most convenient single parameter, the d-band center (ε_d), which is defined as the average energy of the entire Pt d band. The calculated ε_d shift from the Fermi level for Pt/Fe is −2.44 eV. This is a down shift of ∼0.64 eV relative to pure Pt(100)-(1 × 1). The closer the ε_d is to the Fermi level, the stronger the oxygen adsorption should be, based on the d-band center model.[45] The *b-h-b* trajectory for O_2 dissociative adsorption in Pt(100)-(1 × 1) shown in Figure 3 yields oxygen in a dissociated state characterized by a stronger binding energy as compared with that of Pt/Fe. Therefore, the relative strengths of the binding of oxygen in Pt/Fe and in Pt(100)-(1 × 1) are consistent with the shifts in their d-band centers. However, the combined weaker adsorption and easy splitting of O_2 in the bimetallic system calls for perspectives other than the use of ε_d because a low lying ε_d for the bimetallic surface should imply higher activation barrier for O_2 dissociation. So, first, on the basis of the PE curve for *b-h-b* in Pt/Fe in Figure 2 and in Pt(100)-(1 × 1) in Figure 3, O_2 is more stable in Pt/Fe near the entrance channel. Only at a point below z = 2.40 Å does O_2 on pure metal become more stable than that of the bimetallic system. This indicates that the greater stabilization of O_2 in the bimetallic system occurs at only a considerable distance from the surface. Therefore, we plot the 2p states of O_2 at z = 2.80 Å for Pt/Fe, where the large stabilization of O_2 is noted as compared with that of the pure metal. Figure 7a shows the 2p states projected on O, and Figure 7b gives the d states projected on Pt in the bimetallic system. In Figure 7a, two main groups of peaks are identified as the spin−split bonding ppπ (π), which fall within the −6.0 to −10.0 eV energy

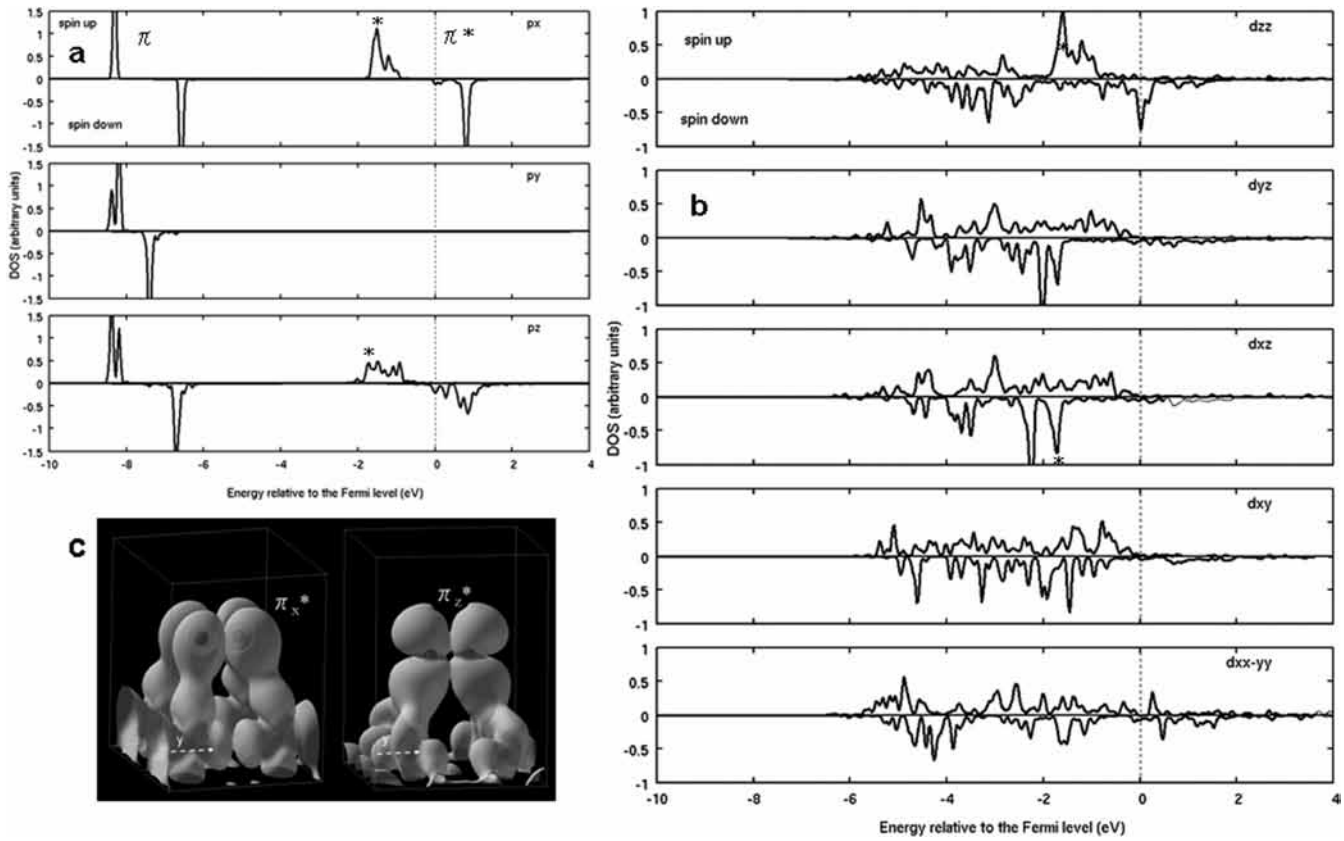

Figure 7. (a) p-DOS projected on O at 2.80 Å from Pt/Fe. Two main groups of peaks are identified as the spin-split bonding ppπ (π) and the antibonding ppπ* (π*). (b) d-DOS projected on Pt. * marks the possible O-2p and Pt-5d hybridizations. (c) Partial charge density plot at Γ for the identified π_x* and π_z* peaks at an isosurface value of 0.0014 and 0.00059 $e^-/Å^3$, respectively.

range, and the antibonding ppπ* (π*), which is within −2 to 2 eV. The Fermi level falls in between the π* gap.

The π states drop out of the Pt d band range so O-2p and Pt-5d hybridization is analyzed only for π* states of oxygen. Here we show the relevant p states that hybridize with corresponding d states of Pt using * marks on Figure 7a,b. On the basis of the O_2 orientation in a *b-h-b* channel in the unit cell (which can also be noted in Figure 6), π_x*−d_{zz} and π_z*−d_{xz} hybridizations are significant in the O-2p and Pt-d states interaction upon the molecule's approach to the surface. Specifically, we note that such are bonding interactions, as shown by the corresponding partial density of states plot at the Γ point in Figure 7c. Between these two bonding interactions, we note the dominant contribution of π_x*−d_{zz} hybridizations because of the intensity of O-2p and Pt-5d states shown in Figure 7a,b. Our previous study on the electronic structure of Pt monolayer on Fe(001) shows an increase in the spin polarization of d_{zz} states at the Fermi level, increasing the d_{zz} vacancy on Pt surface.[20] Therefore, the greater stabilization of O_2 as it approaches the surface in Pt/Fe is traced to the enhanced π_x*−d_{zz} hybridizations in the bimetallic system. Most likely, such interaction could be dominated by an efficient donation to the empty d_{zz} orbital. Only upon reaching considerable distance from the surface (for instance, 2.40 Å, as seen from the 1D PES plots) does back-donation to the antibonding states play the dominant role in the strength of O_2 binding on surface. The increase in d vacancy in Pt/Fe contributes to its inefficiency in back-donation to O_2 antibonding states, as compared with that of the pure metal. Therefore, O_2 is more stable on Pt(100)-(1 × 1) beyond this point up to the most stable dissociated O adsorption on the surface. This increase in d vacancy on Pt on Fe is consistent with the experimentally observed positive chemical shift of the core orbitals of Pt skin on the Pt−Fe alloy surface.[11]

4. Conclusions

We performed spin-polarized first principles calculations to investigate the adsorption and dissociation of O_2 on Pt monolayer on Fe(001). The energetics of O_2 adsorption and dissociation are discussed in terms of the 6D PES. Results show two channels for O_2 adsorption: a molecular adsorption in a top-bridge-top (*t-b-t*) configuration and a translation toward *b-h-b* (surface dissociation mechanism) and a direct dissociative adsorption in a bridge-hollow-bridge (*b-h-b*) channel (direct dissociation mechanism). The latter is proposed to be the most likely pathway for O_2 dissociation. Interestingly, the same reaction pathway is also noted in Pt(100)-(1 × 1), which is consistent with MBE results. However, the activation barriers for O_2 dissociation in Pt/Fe and Pt(100)-(1 × 1) differ significantly. Despite the stronger dissociated O atom binding on Pt(100)-(1 × 1), the activation barrier for O_2 dissociation in this system is still higher compared with Pt/Fe. Therefore, the significant enhancement in electrocatalytic activity of Pt-enriched Pt−Fe alloy is attributed to the unique combination of easy O_2 activation and weaker O atom binding on the surface. We attribute the stabilization of O_2 as it approaches the surface to the enhanced π_x*−d_{zz} hybridizations, which are traced to the increase in Pt d_{zz} vacancy. Such changes in the electronic structure due to Pt interaction with Fe are consistent with the experimentally observed positive chemical shift of Pt core orbitals. Specifically, the π_x* interaction with the empty d_{zz} orbital could be facilitated by enhanced electron donation to the Pt surface near the entrance channel and, upon further

approach of O_2 to the surface (at ~2.4 Å from Pt surface), does back-donation to the antibonding states and becomes more effective in pure metal, and hence the dissociated O is more bound to this system.

Acknowledgment. This work is supported by the "Research and Development of Polymer Electrolyte Fuel Cell Systems" project of the New Energy and Industrial Technology Development Organization (NEDO) and Special Coordination Funds for the Global Center of Excellence (COE) program (H08) "Center of Excellence for Atomically Controlled Fabrication Technology". Some of the calculations were done using computer facilities of the Cyber Media Center (Osaka University), the ISSP Super Computer Center (University of Tokyo), the Yukawa Institute (Kyoto University), and the Japan Atomic Energy Agency (ITBL, JAEA). M.C.S.E. would like to extend gratitude to the SATO International Scholarship Foundation (SISF) for financial support.

References and Notes

(1) Gasteiger, H. A.; Kocha, S. S.; Sompalli, B.; Wagner, F. T. *Appl. Catal., B* **2005**, *56*, 9–35.
(2) Nørskov, J. K.; Rossmeisl, J.; Logadottir, A.; Lindqvist, L.; Kitchin, J. R.; Bligaard, T.; Jonsson, H. *J. Phys. Chem. B* **2004**, *108*, 17886.
(3) Jalan, V.; Taylor, E. J. *J. Electrochem. Soc.* **1983**, *130*, 2299.
(4) Mukurjee, S.; Srinivasan, S.; Soriaga, M. P.; McBreen, J. *J. Electrochem. Soc.* **1995**, *142*, 1409.
(5) Toda, T.; Igarashi, H.; Uchida, H.; Watanabe, M. *J. Electrochem. Soc.* **1999**, *146*, 3750.
(6) Xu, Y.; Ruban, A. V.; Mavrikakis, M. *J. Am. Chem. Soc.* **2004**, *126*, 4717–4725.
(7) Antolini, A.; Salgado, J. R. C.; Gonzalez, E. *J. Power Sources* **2006**, *160*, 957–968.
(8) Stamenkovic, V.; Mun, B. S.; Mayhofer, K.; Ross, P.; Markovic, N.; Rossmeisl, J.; Greeley, J.; Nørskov, J. *Angew. Chem., Int. Ed.* **2006**, *45*, 2897–2901.
(9) Stamenkovic, V.; Mun, B. S.; Arenz, M.; Mayrhofer, K. J. J.; Lucas, C. A.; Wang, G.; Ross, P. N.; Markovic, N. M. *Nat. Mater.* **2007**, *6*, 241.
(10) Mukerjee, S.; Srinivasan, S. *J. Electroanal. Chem.* **1993**, *357*, 201–224.
(11) Toda, T.; Igarashi, H.; Watanabe, M. *J. Electroanal. Chem.* **1998**, *460*, 258–262.
(12) Adzic, R. R. *Electrocatalysis*; VCH: New York, 1998; Vol. 5, p 197.
(13) Clouser, S. J.; Huang, J. C.; Yeager, E. *J. Appl. Electrochem.* **1993**, *23*, 597.
(14) Yeager, E.; Razaq, M.; Gervasio, D.; Razaq, A.; Tryk, D. *J. Serb. Chem. Soc.* **1992**, *57*, 819.
(15) Sidik, R. A.; Anderson, A. B. *J. Electroanal. Chem.* **2002**, *528*, 69.
(16) Ruban, A. V.; Skriver, H. L.; Nørskov, J. K. *Phys. Rev. B.* **1998**, *59*, 15990.
(17) Udaykumar, A.; Mavrikakis, M. *Surf. Sci.* **2008**, *602*, 89–94.
(18) Nørskov, J. K.; Bligaard, T.; Logadottir, A.; Bahn, S.; Hansen, L. B.; Bollinger, M.; Bengaard, H.; Hammer, B.; Sljivancanin, Z.; Mavrikakis, M.; Xu, Y.; Dahl, S.; Jacobsen, C. J. H. *J. Catal.* **2002**, *209*, 275.
(19) Kitchin, J. R.; Nørskov, J. K.; Barteau, M. A.; Chen, J. G. *J. Chem. Phys.* **2004**, *120*, 21.
(20) Escaño, M. C.; Nguyen, T. Q.; Nakanishi, H.; Kasai, H. *Surf. Sci.* **2008**, *602*, 3415.
(21) Escaño, M. C.; Nakanishi, H.; Kasai, H. *J. Phys.: Condens. Matter* **2007**, *19*, 482002.
(22) Hohenberg, P.; Kohn, W. *Phys. Rev.* **1964**, *136*, B864.
(23) Kohn, W.; Sham, L. J. *Phys. Rev.* **1965**, *140*, A1133.
(24) Blöchl, P. E. *Phys. Rev. B* **1994**, *50*, 17953.
(25) Kresse, G.; Joubert, J. *Phys Rev. B* **1999**, *59*, 1758.
(26) Kresse, G.; Furthmüller, J. *Comput. Mater. Sci.* **1996**, *6*, 15.
(27) Kresse, G.; Furthmüller, J. *Phys. Rev. B* **1996**, *54*, 11169.
(28) Kresse, G.; Hafner, J. *Phys. Rev. B* **1993**, *47*, 558.
(29) Kresse, G.; Hafner, J. *Phys. Rev. B* **1994**, *49*, 14251.
(30) Jiang, D. E.; Carter, E. A. *Phys. Rev. B* **2003**, *67*, 214103.
(31) Perdew, J. P.; Burke, K.; Ernzerhof, M. *Phys. Rev. Lett.* **1996**, *77*, 3865.
(32) Perdew, J. P.; Burke, K.; Ernzerhof, M. *Phys. Rev. Lett.* **1997**, *78*, 1396.
(33) Moroni, E. G.; Kresse, G.; Hafner, J.; Furthmüller, J. *Phys. Rev. B* **1997**, *56*, 15629.
(34) Methfessel, M.; Paxton, A. *Phys. Rev. B* **1989**, *40*, 3616.
(35) Eichler, A.; Mittendorfer, F.; Hafner, J. *Phys. Rev. B* **2000**, *62*, 4744.
(36) Kresse, G.; Furthmüller, J. *Phys. Rev. B* **1996**, *54*, 11169.
(37) *CRC Handbook of Chemistry and Physics*, 86th ed.; CRC Press: Boca Raton, FL, 2005.
(38) Ge, Q.; Hu, P.; King, D. A.; Lee, M. H.; White, J. A.; Payne, M. C. *J. Chem. Phys.* **1997**, *106*, 1210.
(39) Deskins, N. A.; Lauterbach, J.; Thomson, K. T. *J. Chem. Phys.* **2005**, *122*, 184709.
(40) Norton, P. R.; Griffiths, K.; Bindner, P. E. *Surf. Sci.* **1984**, *138*, 125–147.
(41) Bradley, J. M.; Guo, X. C.; Hopkinson, A.; King, D. A. *J. Chem. Phys.* **1996**, *104*, 11.
(42) Norton, P. R.; Binder, P. E.; Griffiths, K. *J. Vac. Sci. Technol., A* **1983**, *2*, 1028.
(43) Griffiths, Jackman, T. E.; Davies, J. A.; Norton, P. R. *Surf. Sci.* **1984**, *138*, 113–124.
(44) Greeley, J.; Mavrikakis, M. *Nat. Mater.* **2004**, *3*, 810–815.
(45) Hammer, B.; Nørskov, J. K. *Surf. Sci.* **1995**, *343*, 211–220.

JP9030267